GROWTH AND CONFIGURATIONAL STABILITY OF CIRCULAR, BUCKLING-DRIVEN FILM DELAMINATIONS

J. W. HUTCHINSON[1], M. D. THOULESS[2] and E. G. LINIGER[2]

[1]Division of Applied Sciences, Harvard University, Cambridge, MA 02138 and [2]IBM Research Division,
Thomas J. Watson Research Center, Yorktown Heights, NY 10598, U.S.A.

Abstract—A study is presented of delamination at the interface between a thin elastic film bonded to a substrate under conditions in which the film is subject to equi-biaxial compression. The focus is on initially circular delaminations. When the initial delamination is sufficiently large it buckles away from the substrate producing a blister which in turn induces a driving force on the interface crack tip. A two-part theoretical analysis of the coupled buckling/fracture problem is conducted: the axisymmetric growth of the circular blister, and the stability of the circular blister to nonaxisymmetric perturbations of the interface crack front. A simple criterion is identified which excludes the possibility of wide-spread delamination. Experiments are reported for a model film/substrate system (mica bonded to aluminum) chosen to allow visualization of the interface and to permit compressive stresses in the film to be generated over the full range of interest by exploiting the large thermal expansion mismatch of the system. The experiments bear out the theoretical prediction of a regime of axisymmetric growth which gives way to nonaxisymmetric blisters after a blister becomes sufficiently large. The study suggests that the wavy-circular and worm-like blister morphologies which are usually observed for delaminated films are a manifestation of the configurational instability of the interface crack front.

Résumé—Nous présentons une étude de la décohésion interfaciale en feuillets entre un film élastique mince et son support, lorsque le film est soumis à une compression équiaxiale. Nous nous intéressons plus précisément aux décohésions qui sont au départ circulaires. Quand la décohésion initiale est suffisamment importante, elle s'éloigne du support en se déformant, ce qui provoque une cloque qui à son tour induit une force motrice sur l'extrémité de la fissure interfaciale. Ce double problème gauchissement/rupture est analysé théoriquement sous les deux aspects suivants: croissance avec un axe de révolution de la cloque circulaire et instabilité de la cloque circulaire vis-à-vis des perturbations sans axe de révolution du front de la fissure d'interface. Nous identifions un critère simple qui exclut la possibilité d'une décohésion à grande échelle. Nous présentons les expériences réalisées sur un système modèle film/support (mica lié à l'aluminium) que nous avons choisi pour pouvoir visualiser l'interface, et pour pouvoir créer des contraintes de compression dans le film, dans tout le domaine intéressant, en exploitant le fort désaccord de dilatation thermique du système. Ces expériences confirment la prévision théorique d'un régime de croissance avec un axe de révolution qui conduit à des cloques sans axe de révolution une fois que ces cloques se sont suffisamment développées. Cette étude suggère que les morphologies de cloques, vaguement circulaires ou en forme de serpentin, que l'on observe dans les films après décohésion sont une manifestation de l'instabilité de la configuration du front de la fissure d'interface.

Zusammenfassung—Es wird die Delamination an de Grenzfläche zwischen einem dünnen elastischen Film und einem Substrat unter Bedingungen untersucht, unter denen der Film unter einem gleichmäßigen biachsialen Druckzustand steht. Analysiert wird eine anfänglich runde Delamination. Ist diese ausreichend groß, dann biegt sie sich von der Grenzfläche weg und bildet einen Hohlraum, einen "Blister", der selbst wiederum eine treibende Kraft auf die Spitze des Risses an der Grenzfläche darstellt. Das Problem der Blisterbildung, gekoppelt mit Bruch, wird zweistufig theoretisch analysiert: dans achsensymmetrische Wachstum der runden Blister und die Stabilität der runden Blister gegenüber nicht-achsensymmetrischen Störungen der Rißfront in der Grenzfläche. Es ergibt sich ein einfaches Kriterium, welches die Möglichkeit ausgedehnter Delamination ausschließt. Experimente an einem Modellsystem (Glimmer auf Aluminium) werden vorgestellt; das system wurde gewählt, um die Grenzfläche sehen zu können und kompressive Spannungen im Film im gesamten interessierenden Bereich über die große thermische Fehlpassung einstelln zu können. Die Experimente bestätigen die theoretischen Voraussagen eines Bereiches achsensymmetrischen Wachstums, welches zur Bildung nicht-achsensymmetrischen Blister führt, wenn ein Blister erst ausreichende Größe erreicht hat. Die Untersuchung legt nahe, daß die wellenförmig-runden und wurmartigen Blistermorphologien, di üblicherweise in delaminierten Filmen beobachtet werden, ein Ausdruck der Konfigurationsinstabilität der Front des Grenzflächenrisses darstellen.

1. INTRODUCTION

A thin elastic film in compression bonded to a substrate will undergo buckling-driven interfacial delamination when the compressive stress is sufficiently high if an initially debonded patch of interface exists.

This type of delamination has been observed for many different film/substrate systems [e.g. 1–4]. The unbuckled film produces no driving force on the interface crack comprising the initial debond patch. Buckling induces a crack driving force which will
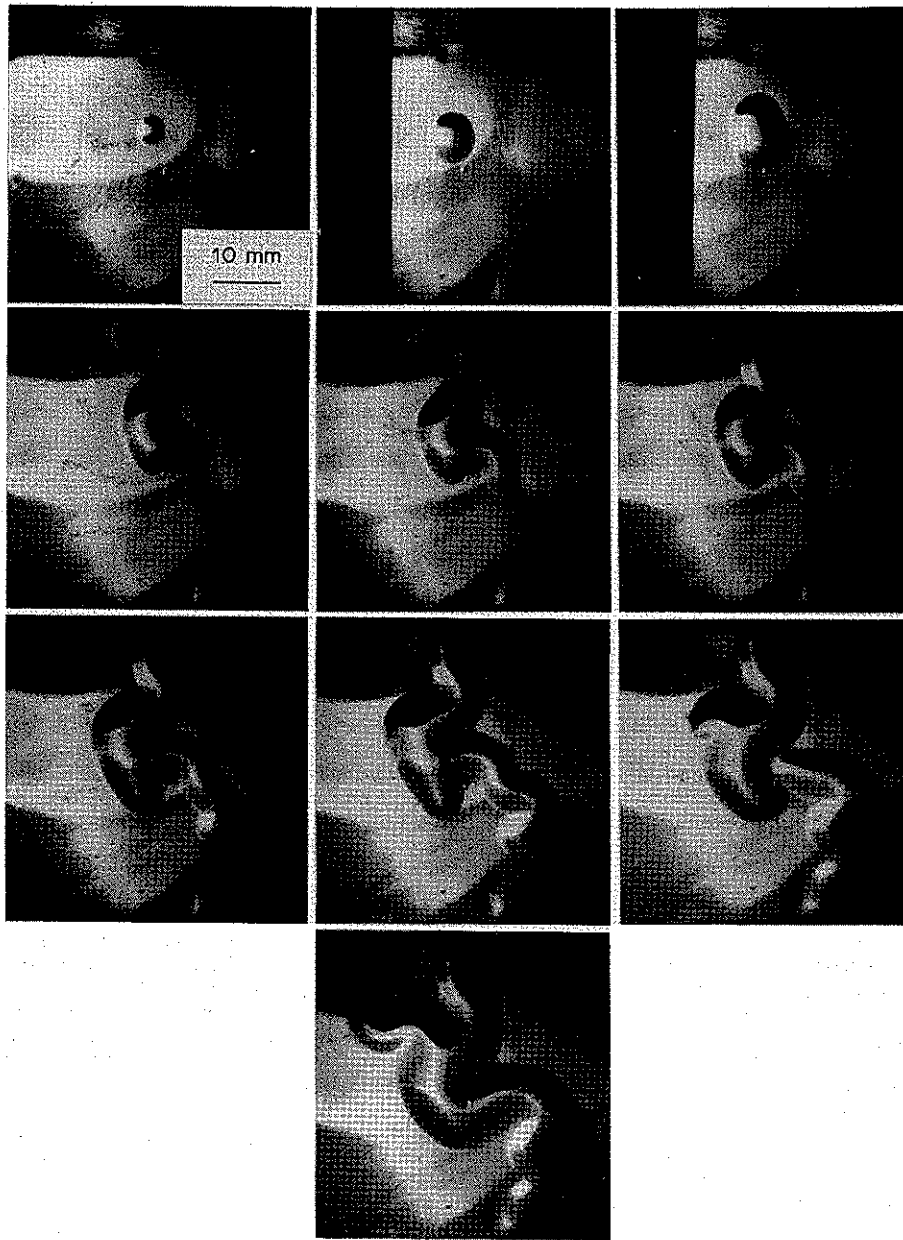
Fig. 1. Sequence of photographs showing growth of an initially circular debonded region under increasing σ.

cause the interface crack to advance if the interface toughness is sufficiently low. Various shapes of buckling-driven delaminations evolve, including long straight-sided blisters, circular blisters with and without wavy edges, and the "worm" or "telephone cord" blisters.

Figure 1 is a sequence of photographs of a delaminated region spreading from an initially circular debonded patch. The system, which will be described fully in Section 4, is a mica film on an aluminum substrate. An equi-biaxial compressive stress state σ is produced in the unbuckled film by lowering the temperature of the system, which has a large thermal

expansion mismatch. The sequence in Fig. 1 shows the spread of the initially circular debond patch under increasing σ. The blister spreads remaining more-or-less circular until a point is reached where it clearly loses its circular symmetry. With further increase in σ the blister turns into a "worm" or "telephone cord" blister.

In the next section, conditions for the axisymmetric spreading of a circular blister are derived. These are followed in the subsequent section by an analysis of the loss of stability of the circular shape to nonaxisymmetric perturbations. The axisymmetric analysis provides a simple criterion for ensuring that

buckling-driven delamination does not occur. This criterion depends on the mixed-mode debond toughness of the interface in an essential way. The predictions for the loss of configurational stability of the circular delamination are in general agreement with the experimental observations reported in Section 4. While the telephone cord blister has not been analyzed in this paper, we believe that the explanation underlying this morphology is closely tied to the issue of configurational instability of the crack front illustrated for the circular blister.

Buckling-driven delamination involves the nonlinear coupling of buckling and fracture. The phenomenon occurs both in thin film/substrate systems and as a compressive failure mode in laminated composites [5–12]. The importance to the phenomenon of the dependence of debond toughness on the combination of mode 1 (tension) and mode 2 (shear) experienced by the debonding interface was first documented in [12] for the case of ply delamination of laminated composites. A common feature to the spread of buckling-driven delaminations, for both one-dimensional blisters in [12] and the circular blisters considered here, is an increase in the relative proportion of mode 2 to mode 1. Thus, the mixed-mode debond toughness of the interface must be accounted for. The study presented here is conducted within the framework of interfacial fracture mechanics which is laid out in [13].

2. AXISYMMETRIC GROWTH OF A CIRCULAR BLISTER

A theoretical analysis of a circular blister in a thin film is presented in this section and the next. The film is assumed to be isotropic with Young's modulus E_1 and Poisson's ratio v_1. It's thickness is h. The substrate is also taken to be isotropic but with different moduli quantities, E_2 and v_2. The substrate is modeled as being infinitely thick. The stress state in the film in the unbuckled state is uniform, equi-biaxial compression σ. The energy release rate and the

measure of the relative proportion of mode 2 to mode 1 of the interface crack for the circular blister is presented in this section, along with conditions for axisymmetric spreading. The stability of the circular blister to nonaxisymmetric perturbations of the interface crack front is analyzed in Section 3.

With reference to Fig. 2(a), consider a circular blister of radius R. A circular interface crack exists on the interface between the film and the substrate such that the film is unbonded for $r \leqslant R$. When the film is unbuckled ($\delta = 0$, where δ is the deflection at $r = 0$), the stress in the film is a uniform state of equal biaxial compression ($\sigma_{rr} = \sigma_{\theta\theta} = -\sigma$). In the unbuckled state the stress intensity factors and energy release rate of the interface crack are zero. Only when the film buckles away from the substrate is there a nonzero crack driving force.

The analysis for the circular blister is summarized in the Appendix, and the results are reported below. Limited results on the same problem have been reported in [9, 10, 13]. The present paper draws on the theory laid out in [13], and the reader will be referred to this reference for certain details of the theory.

Under the assumption that $R/h \gg 1$, the buckled film is modeled as a completely clamped circular plate governed by von Karman nonlinear plate theory. A clamped circular plate buckles in an axisymmetric mode. The ciritical stress when the plate just begins to buckle away from the substrate is

$$\sigma_c = 1.2235 \frac{E_1}{1 - v_1^2} \left(\frac{h}{R}\right)^2. \qquad (1)$$

For stresses in excess of σ_c the film buckles away from the substrate such that

$$\frac{\delta}{h} \cong \left[\frac{1}{c_1}\left(\frac{\sigma}{\sigma_c} - 1\right)\right]^{1/2} \qquad (2)$$

where $c_1 = 0.2473 (1 + v_1) + 0.2231 (1 - v_1^2)$. This result is asymptotically exact for σ just above σ_c, but it remains a fairly good approximation for large σ/σ_c. For $v_1 = 1/3$, it overestimates δ/h by 7% when $\sigma/\sigma_c = 10$ and by 25% when $\sigma/\sigma_c = 50$.
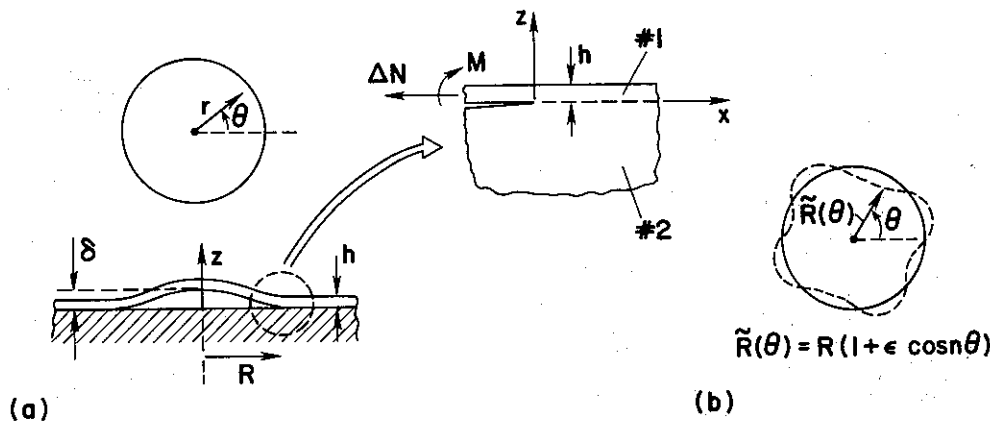

Fig. 2. (a) Conventions for axisymmetric blister and plane strain problem at edge of the interface crack. (b) Perturbation of the circular interface crack front.

2.1. The edge-crack solution

The energy release rate and stress intensity factors of the interface crack are obtained by coupling the buckled plate solution to the solution to the plane strain edge-crack problem shown in Fig. 2(a). This problem, which was originally solved in [14], involves an edge-crack separating the film and an infinitely deep substrate with loadings M (moment/unit length of crack edge) and ΔN (resultant stress-force/unit length of crack edge) acting on the film with the sign conventions shown. These quantities will be identified with the moment/unit length ($M \equiv M_{rr}$) and the resultant stress *change* ($\Delta N \equiv N_{rr} + \sigma h$, where N_{rr} is the standard notation for the resultant radial inplane stress) at the edge of the buckled plate.

The plane strain solution [14] to the edge-crack problem involves the two Dundurs' elastic mismatch parameters

$$\alpha = (\bar{E}_1 - \bar{E}_2)/(\bar{E}_1 + \bar{E}_2) \qquad (3)$$

and

$$\beta = \tfrac{1}{2}[(\mu_1(1 - 2v_2) - \mu_2(1 - 2v_1)]/$$
$$[\mu_1(1 - v_2) + \mu_2(1 - v_1)] \qquad (4)$$

where $\bar{E}_i = E_i/(1 - v_i^2)$ and $\mu_i = E_i/[2(1 + v_i)]$ for $i = 1, 2$. Note that α and β both vanish in the absence of any mismatch. Generally, α is the more important of the two parameters for interfacial fracture problems. Moreover, a non-zero β-value complicates somewhat the application of interfacial fracture mechanics. In this paper, attention will be restricted to mismatches with $\beta = 0$, either exactly or by approximation. Nothing of essence in the blister problem is lost by taking $\beta = 0$. The effect of non-zero β is included in the treatment given in [13].

With $\beta = 0$, the normal and shear stresses on the interface a distance x ahead of the crack tip are controlled by the mode 1 and mode 2 stress intensity factors, K_1 and K_2, in the usual way according to $\sigma_{zz} = K_1(2\pi x)^{-1/2}$ and $\sigma_{xz} = K_2(2\pi x)^{-1/2}$. The energy release rate for straight-ahead propagation of the interface crack is related to the intensity factors by

$$G = (K_1^2 + K_2^2)/E_* \qquad (5)$$

where $1/E_* = 1/2(1/\bar{E}_1 + 1/\bar{E}_2)$ when $\beta = 0$.

For the edge-crack problem [14]

$$G = \frac{6(1 - v_1^2)}{E_1 h^3}\left(M^2 + \frac{1}{12} h^2 \Delta N^2\right) \qquad (6)$$

and

$$\tan \psi \equiv \frac{K_2}{K_1} = \frac{\cos \omega + [h\Delta N/(\sqrt{12}\, M)]\sin \omega}{-\sin \omega + [h\Delta N/(\sqrt{12}\, M)]\cos \omega} \qquad (7)$$

where $\omega(\alpha)$ is plotted in Fig. 3. Throughout the paper, ψ will be used to measure the relative proportion of mode 2 to mode 1. Since $K_1 = (E_*G)^{1/2} \cos \psi$ and $K_2 = (E_*G)^{1/2} \sin \psi$, G and ψ fully characterize the plane strain crack tip field at the edge of the circular blister.
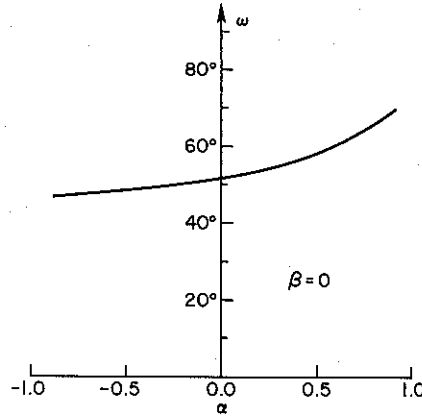

Fig. 3. Dependence of ω in (7) on elastic mismatch parameter for $\beta = 0$.

2.2. G and ψ for the circular blister

The elastic energy per unit area stored in the unbuckled film is

$$G_0 = (1 - v_1)h\sigma^2/E_1 \qquad (8)$$

The energy release rate, G, is obtained from (6) using the moment and resultant stress change quantities at the edge of the buckled clamped plate. The ratio G/G_0 depends only on σ/σ_c and v_1, and this ratio is plotted in Fig. 4 for three values of v_1. These results are based on a full numerical analysis as described in the Appendix. An asymptotically exact result for $\sigma/\sigma_c \to 1$ is [13]

$$G/G_0 = c_2[1 - (\sigma_c/\sigma)^2] \qquad (9)$$

where $c_2 = [1 + 0.9021(1 - v_1)]^{-1}$. This expression retains its accuracy for σ/σ_c up to about 2.

As seen in Fig. 4, G increases monotonically with σ/σ_c, slowly approaching G_0. By (1), the sole loading parameter is

$$\frac{\sigma}{\sigma_c} = 0.8173(1 - v_1^2)\frac{\sigma}{E_1}\left(\frac{R}{h}\right)^2. \qquad (10)$$

Thus, σ/σ_c can increase due either to an increase in blister radius, R, or to an increase in the unbuckled film stress σ.
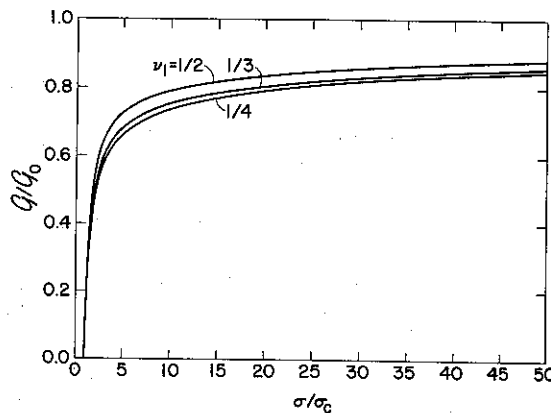

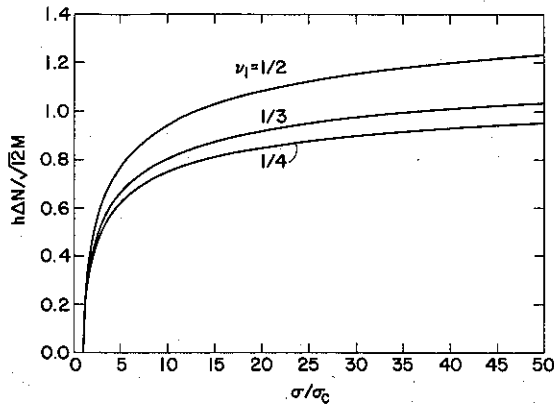Fig. 4. Normalized energy release rate for axisymmetric blister.

Fig. 5. Ratio of load quantities at the edge of the circular blister needed in (7) to predict the measure of mode mixity ψ.

From (7) it can be seen that ψ depends on the elastic mismatch through $\omega(\alpha)$ and on the conditions at the edge of the buckled plate only through the combination of terms $h\Delta N/(\sqrt{12}\,M)$. This combination, which also is only a function of σ/σ_c and ν_1, is plotted in Fig. 5. The asymptotic expression, which is accurate for σ/σ_c up to 2, is

$$h\Delta N/(\sqrt{12}\,M) = 0.2486(1 + \nu_1)(\delta/h) \qquad (11)$$

where δ/h is given by (2). The results in Fig. 5 are combined with (7) to generate the curves of ψ vs σ/σ_c in Fig. 6. For σ/σ_c emerging from 1, ψ starts at $\omega - \pi/2$. In the absence of any mismatch ($\alpha = 0$), $\omega = 52.1°$ and ψ starts at $-37.9°$. As σ/σ_c increases, $|\psi|$ increases with the interface crack tip becoming more heavily mode 2 compared to mode 1. This trend underlies the delamination behavior of a circular blister, as will now be discussed.

2.3. Mode-dependent interface toughness and crack driving force

Recent experimental studies on the fracture of interfaces [15–19] have established a significant mode-dependence of the interface toughness of a number of relatively brittle interfaces. When time-dependent effects can be ignored, the criterion for incipient advance of an interface crack under combined mode 1/mode 2 conditions is

$$G = \Gamma(\psi). \qquad (12)$$

The experimental studies have shown that the interface toughness, $\Gamma(\psi)$, increases with increasing $|\psi|$. In the case of an epoxy-glass interface [18], nearly a tenfold increase in Γ has been observed from mode 1 ($\psi = 0°$) to near-mode 2 ($\psi \cong \pm 90°$).

Mode-dependence of interface toughness plays an essential role in the blistering failure mode. Suppose the "classical" mode-independent criterion, $G = \Gamma_{1c}$, were in effect. Then, because G increases monotonically with σ/σ_c (cf. Fig. 4), the blister would spread without limit once the condition $G = \Gamma_{1c}$ was first reached at its edge. In other words, a blister would

either be sub-critical with $G < \Gamma_{1c}$ or the film would completely delaminate. This is clearly not in accord with the wide variety of stable morphologies observed to have spread from smaller blisters. The observed behavior is tied to the increase in relative proportion of mode 2 to mode 1 displayed in Fig. 6 coupled with a mode-dependent interface toughness $\Gamma(\psi)$.

For the purpose of theoretical modeling it is useful to have a phenomenological representation for $\Gamma(\psi)$. Here we will use [13, 19]

$$\Gamma(\psi) = \Gamma_{1c}\,f(\psi) \qquad (13)$$

where Γ_{1c} is the mode 1 toughness and

$$f(\psi) = 1 + \tan^2[(1 - \lambda)\psi]. \qquad (14)$$

This is a one-parameter family of toughness functions. For $\lambda = 1$ it coincides with the classical mode-independent criterion $G = \Gamma_{1c}$, while for $\lambda = 0$ it reduces to a criterion based on a critical value of K_1, independent of K_2, i.e. $K_1 = (E_*\Gamma_{1c})^{1/2}$. The interface toughness functions are plotted in Fig. 7(a), and the ratio of mode 2 to mode 1 toughness is plotted as a function of the parameter λ in Fig. 7(b). The data for the epoxy/glass interface [18] is modeled by (14) with a value of λ of about 0.2, while data for a brittle wax/glass interface over the range, $0 \leqslant \psi \leqslant 37°$, corresponds to $\lambda \cong 0$ [16]. A micro-mechanics model of interface toughness based on asperity interaction [20] gives rise to a family of functions similar to (14) where λ is related to the roughness of the fractured interface.

For discussing and presenting results it is also useful to define *a mode-adjusted crack driving force*

$$F = G/f(\psi) \qquad (15)$$

such that the condition for incipient fracture (12) becomes simply

$$F = \Gamma_{1c}. \qquad (16)$$

This force quantity is also central to the discussion of configurational instability. Plots of the non-dimensional mode-adjusted crack driving force for the
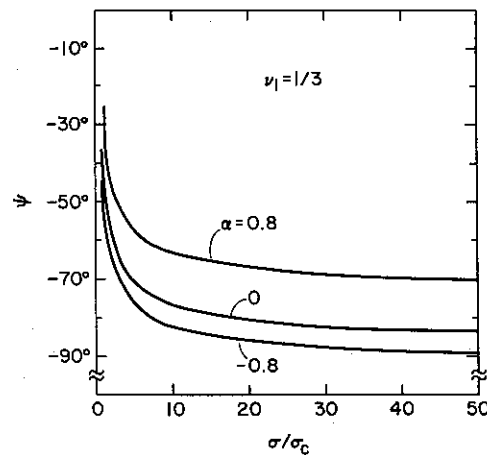

Fig. 6. Mode mixity parameter ψ vs σ/σ_c for three levels of elastic mismatch between film and substrate for circular blister.

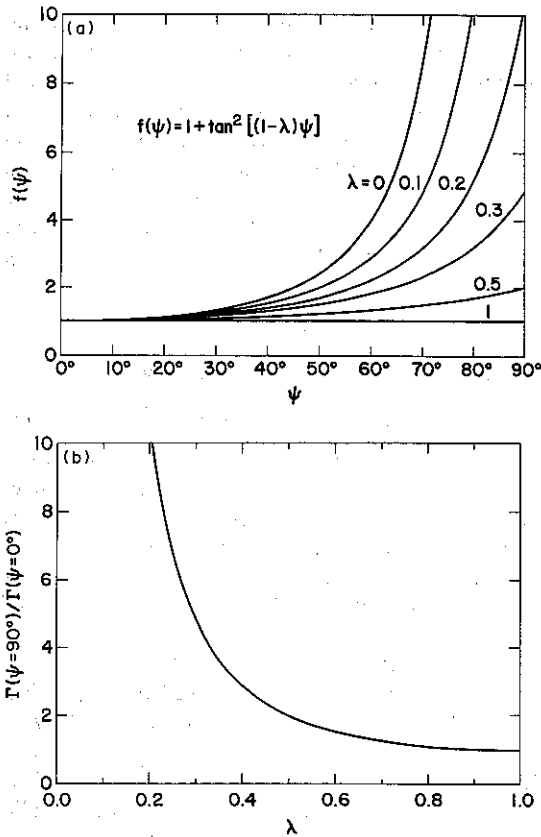$$f(\psi) = 1 + \tan^2\left[(1-\lambda)\psi\right]$$

Fig. 7. (a) Family of interface toughness functions. (b) Ratio of toughnesses in pure mode 2 to pure mode 1 as dependent on λ.

circular blister are shown in Fig. 8 for $\alpha = 0$ and $v_1 = 1/3$.

2.4. Spreading of a circular blister

The plots of mode-adjusted crack-driving force show that, above a certain value of σ/σ_c, F diminishes with increasing σ/σ_c, assuming $\lambda < 1$. Thus, by (16), a spreading circular blister in a state to the right of a maximum in Fig. 8 is stable, except for the possibility of instability with respect to nonaxisymmetric growth discussed in the next sub-section. A better
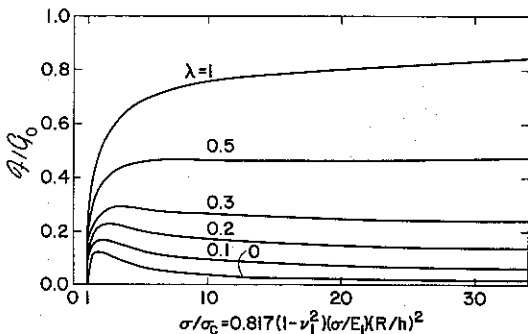

Fig. 8. Mode-adjusted crack driving force at edge of circular blister vs σ/σ_c for the family of interface toughness functions shown in Fig. 7 with $\alpha = 0$ and $v_1 = 1/3$. The condition for incipient crack advance is $F = \Gamma_{1c}$.
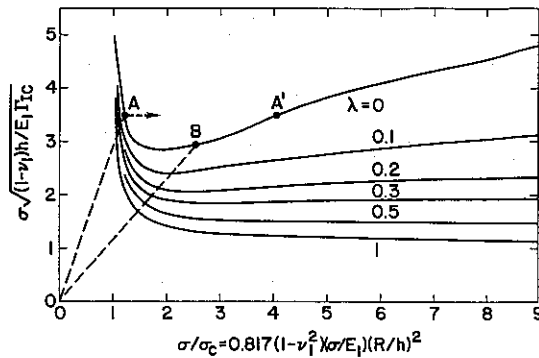

Fig. 9. Normalized stress associated with incipient spread of the circular blister for the family of interface toughness functions shown in Fig. 7 with $\alpha = 0$ and $v_1 = 1/3$.

plot for revealing the parameters controlling the blister is obtained by rewriting the fracture criterion, $G = \Gamma(\psi)$, with the aid of (8), (13) and (15) as

$$\sigma\left[\frac{(1-v_1)h}{E_1\Gamma_{1c}}\right]^{1/2} = \left(\frac{G_0}{F}\right)^{1/2}. \qquad (17)$$

The right hand side of this equation is a function of σ/σ_c (cf. Fig. 8), and plots of this condition for crack advance are given in Fig. 9 for the choice of $f(\psi)$ given in (14) with $\alpha = 0$ and $v_1 = 1/3$.

For the purpose of discussion, focus on the curve for $\lambda = 0$ in Fig. 9. Suppose an initial circular debond region exists, and suppose the film thickness h is fixed with the film loaded by increasing σ. This loading corresponds to a straight line trajectory in Fig. 9. If the parameters of the system are such that the trajectory is one like OA, which intersects the curve for crack advance to the *left* of the minimum, then the blister will undergo unstable (dynamic) advance until it is arrested at A', neglecting any dynamic overshoot. With further increase of σ the interface crack advances stably, with σ/σ_c increasing. If, however, the trajectory is like OB, intersecting the propagation curve to the *right* of the minimum, the spreading process is stable from the start. Similar interpretations apply if σ is fixed and h increases, as in a film deposition process, but the loading trajectories are no longer straight lines.

Let $y(\lambda)$ denote the minimum of the propagation curve in Fig. 9 for a given λ. There will be no blister spreading *regardless of the size of the initial debond region* if

$$\sigma\left[\frac{(1-v_1)h}{E_1\Gamma_{1c}}\right]^{1/2} < y(\lambda). \qquad (18)$$

This limit may be useful in the design or deposition of compressed thin films since it ensures that widespread delamination will not occur, at least not as circular blisters. This is an overly conservative criterion in the sense that it underestimates the stress (or thickness) a film can tolerate when initial debond regions are small. Noting that the minima in Fig. 9 are approximately attained at $\sigma/\sigma_c \cong 2$, it follows

from (10) that a small initial debond in this context is one which satisfies $R \ll R^*$ where

$$R^* \cong 1.5\, h \left(\frac{E_1}{(1 - v_1^2)\sigma} \right)^{1/2}$$

$$= 1.5\, h \left[\frac{(1 - v_1)E_1 h}{y^2(1 - v_1^2)^2 \Gamma_{1c}} \right]^{1/4}. \quad (19)$$

When the radius of the initial debond is comparable to R^* the criterion (18) pertains without a cushion of conservatism.

By examining the numerical results in Fig. 9 and similar results based on other choices of $f(\psi)$, such as those discussed in [13], we have observed that the following rough approximation holds: $\Gamma_{1c} y(\lambda)^2 \cong \Gamma(\psi = -70°)$. Thus, (18) can be rewritten (approximately) as

$$(1 - v_1)h\sigma^2/E_1 < \Gamma(\psi \cong -70°). \quad (20)$$

The results in [13] for the steady-state propagation of straight-sided blisters leads to a condition for excluding that mode of delamination which is quantitatively similar. In this form the interpretation of the criterion for the exclusion of wide-spread delamination is very simple. It states that wide-spread delamination will not occur as long as the strain energy per unit area stored in the film is less than the interface toughness associated with the mode mixity, $\psi \cong -70°$.

3. CONFIGURATIONAL STABILITY OF THE CIRCULAR BLISTER

Two possibilities have been considered to explain the tendency for the circular blister to develop a non-circular shape. The first possibility analyzed was nonaxisymmetric buckling from the nonlinear axisymmetric state when the interface crack front remains circular. The bifurcation analysis reported in the Appendix reveals that bifurcation into a non-axisymmetric mode does not occur until $\sigma/\sigma_c = 55.6$ for $v_1 = 1/3$. The θ-variation of the lowest mode is of the form $\cos n\theta$ with $n = 8$. Since distinct nonaxisymmetric behavior is observed at values of σ/σ_c in the vicinity of 5, it is concluded that such behavior is *not* a result of nonaxisymmetric buckling.

The second possible source of nonaxisymmetric behavior considered was instability to non-circular perturbations of the circular crack front. With the notation introduced in Fig. 2(b), perturbations in the crack front were considered in the form.

$$\tilde{R}(\theta) = R(1 + \epsilon \cos n\theta) \quad (21)$$

where ϵ is the perturbation parameter. Configurational instability of this kind is clearly evident in

---

†Large nonaxisymmetric perturbations of the crack front will induce a mode 3 contribution to the energy release rate. However, to the lowest order in ϵ, the mode 3 contribution vanishes and consequently the criterion based on (15) and (16) still holds.

---

delaminations presented in [2] and will be further discussed in connection with the experiments reported in Section 4. Before describing the analysis and its outcome, we give a qualitative explanation for the tendency for the crack front to be unstable to perturbations along its length. We believe that this explanation also lies at the heart of why worm-like telephone cord blisters are so frequently observed.

First note again that the mode-adjusted crack driving force diminishes with increasing R beyond the peak value in Fig. 8. The peak in F occurs when σ/σ_c is roughly 2 for λ in the range 0 to 0.3, and thus F diminishes with increasing R for values greater than about R^* given in (19). This trend already hints at the fact that a perturbation with a higher curvature (i.e. a lower local radius of curvature R) will have a higher local driving force than the average once the blister radius is well in excess of R^*. A more convincing clue comes from a comparison of the driving force for the circular blister to that of an infinite straight-sided blister. The straight-sided blister problem can be solved in closed form. We have used the results from [13] to calculate F along the straight crack edge of a straight-sided blister of half width b, and in Fig. 10 we have plotted the ratio of F for the circular blister to F for the straight-sided blister. The abscissa in this plot used L as the measure of blister size, where $L = R$ for the circular blister and $L = b$ for the straight-sided blister. From Fig. 10 one sees that below a certain size, which depends on λ, the driving force for the straight crack front exceeds that of the curved front, but above that size the curved crack front develops a substantially larger driving force. This occurs because the relative proportion of mode 2 to mode 1 increases more slowly for the circular blister than for the straight-sided blister as they expand (compare Fig. 6 with Fig. 6.5 of [13]). Thus, beyond a certain size, a curved crack front experiences a higher driving force than one that is straight, and perturbations which take advantage of this tendency will tend to be enhanced.

The detailed analysis of the stability of the crack front of the circular blister, which is described in the Appendix, provides the lowest order perturbation in the mode-adjusted crack driving force F defined in (15). The result of the analysis has the form

$$F = F_0(\sigma/\sigma_c) + \epsilon F_1(\sigma/\sigma_c, n) \cos n\theta \quad (22)$$

where F_0 is the value of F in the axisymmetric state and F_1 is the Fourier coefficient associated with the lowest order perturbation. Both F_0 and F_1 depend on the choice of $f(\psi)$ and on the elastic mismatch parameters in addition to the other dependencies indicated.

Stability with respect to a perturbation of the crack front with a given n hinges on the sign of F_1. The propagation criterion along the crack front is the maintenance of a constant F according to $F = \Gamma_{1c}$.† Thus if F_1 is *negative* for a given n, the perturbation is *stable* in the sense that the outward excursions of
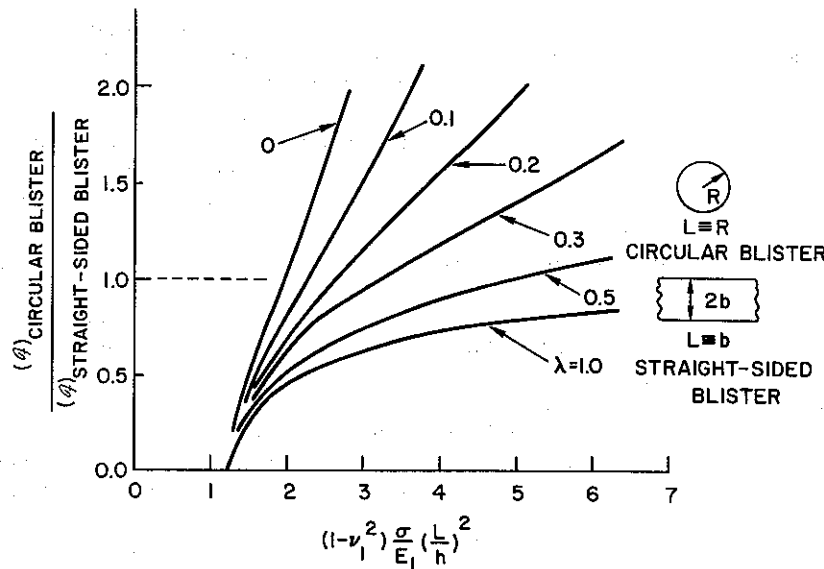
Fig. 10. Ratio of mode-adjusted crack driving force for a circular blister to that for the straight edge of a straight-sided blister at comparable sizes and at the same level of equi-biaxial compression in the film.

the crack front lower F relative to the innermost points along the front. The crack will resume its circular shape as it expands. Conversely, if F_1 is *positive* the outward excursions experience the higher F-values and the perturbation is *unstable*. The crack will be driven further away from the circular shape as it expands.

Curves of F_1/G_0 as a funtion of σ/σ_c are plotted in Fig. 11(a) for $n = 2, 8$ for the case $\lambda = 0$ with no elastic mismatch. To lowest order in ϵ, the solution for $n = 1$ corresponds to a simple translation without distortion of the debonded region giving $F_1 = 0$, which is of no particular interest. The value of σ/σ_c at which each mode becomes unstable is indicated by a solid dot in Fig. 11(b). In this same figure the range of σ/σ_c is shown in which F_1 for the given mode is larger than that for any of the other modes. It is expected that a given mode is most likely to be observed within this range, assuming another morphology does not set in. Results for the values of σ/σ_c at which the modes first become unstable are shown in Fig. 12 for various λ with $\alpha = 0$ and for $\lambda = 0$ with two other elastic mismatches. It can be seen that the instability transition is only weakly dependent on λ and α.

The first nonaxisymmetric instability occurs for $n = 2$ with σ/σ_c in the range 5–9, depending on the elastic mismatch and on λ. Note that this instability point occurs well to the right of the minima of the curves in Fig. 9. It follows, therefore, that the condition limiting blister spreading given by (18) or (19) is not invalidated by the transition to nonaxisymmetric blisters.

4. EXPERIMENTS

In an attempt to illustrate some of the concepts discussed in the previous sections, a series of model

experiments was devised. The system chosen for these experiments consisted of a thin mica sheet bonded to an aluminum substrate by means of a thermoplastic resin.† The difference in the coefficients of thermal expansion between the aluminum and mica was used to induce a residual compressive stress in the mica.
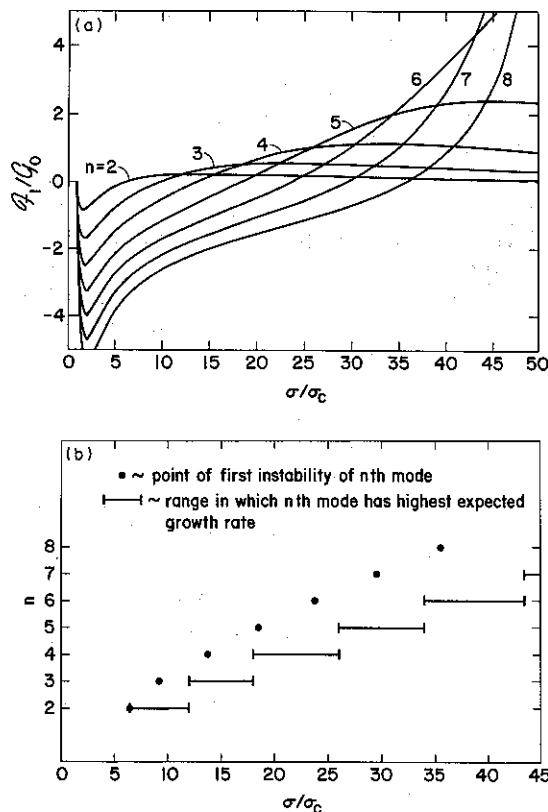

† Buehler Lakeside-80 Thermoplastic Cement.

Fig. 11. (a) F_1/G_0 vs σ/σ_c for $\lambda = 0$ with $\alpha = 0$ and $\nu_1 = 1/3$. (b) Mode instability plot for $\lambda = 0$ with $\alpha = 0$ and $\nu_1 = 1/3$.
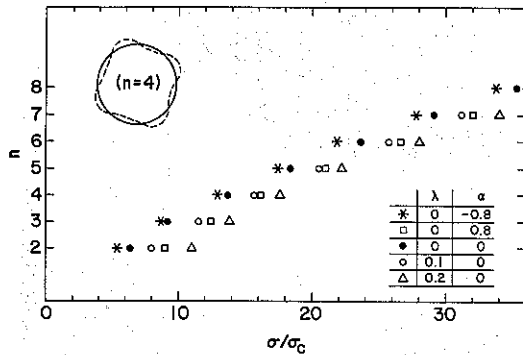
Fig. 12. Onset of instability of modes for various λ with $\alpha = 0$ and for $\lambda = 0$ for $\alpha = \pm 0.8$, all with $v_1 = 1/3$.

The magnitude of this stress was controlled by varying the temperature of the composite system. An important feature of these experiments was that a controlled flaw could be introduced into the interface between the mica and the resin (where all delamination events subsequently took place) by means of a screw threaded through the back face of the substrate (Fig. 13). This technique had an additional advantage in that it ensured that any possible effects of atmospheric pressure on the buckling and delamination were eliminated.

Mica was chosen for the film because it could be obtained in large (150 mm × 150 mm), uniform sheets that were thin enough (14–130 μm) to be suitably flexible for the experiments. Aluminum was selected for the substrate because of its high coefficient of thermal expansion and its good thermal conductivity. The Dundurs' elastic-mismatch parameters, α and β, for mica and aluminum are approximately 0.4 and 0.1 respectively. Reference [13] shows that, for these values of α and β, the value of ω in (7) is almost identical to $\omega(\alpha = 0, \beta = 0)$. Therefore, although the elastic-mismatch parameters are non-zero for mica and aluminum, it is appropriate to analyze such a combination using the results for a homogeneous system.

An essential piece of knowledge that was required before any quantitative information could be ob-

tained from these experiments was a reference temperature below which elastic stresses were not relieved by the resin. This temperature was determined to be $52 \pm 2°C$ by an experiment in which the resin was used to fabricate a composite beam from two different materials. When the beam was cooled to room temperature, it bent under the action of the residual stresses induced by the difference in thermal expansion between two materials. The curvature, which was measured by means of optical interferometry, was used to deduce the residual stress and, hence, the reference temperature.

In the main portion of this study, two sets of experiments were performed to investigate the buckling and delamination phenomenon. In one set, the buckling parameter, σ/σ_c, was varied by holding σ constant but decreasing σ_c by progressively increasing the flaw size. In the second set of experiments, which better approximated the assumptions of the theoretical modeling, the magnitude of σ was increased by cooling the samples on a cold stage.

In the first group of experiments, the composite system was cooled to room temperature; the biaxial compressive stress in the mica was therefore about 100 MPa. An approximately circular delamination was introduced by means of the screw which was subsequently removed. The size and shape of the resulting blister were determined, and the screw was then reinserted so as to increase the size of the delamination. The process was repeated to obtain a range of observations from a single sheet of mica. Typical micrographs of the blisters are shown in Fig. 14; the nonaxisymmetric nature of the delamination can be seen clearly. The results are summarized in Fig. 15 in which the number of nodes observed for each blister is plotted as a function of σ/σ_c for four different sheets of mica. The mean value of the radius of the blister was used to estimate σ_c, and the error bars in Fig. 15 give an indication of the uncertainty in the values. A comparison of this figure with Figs 11 and 12 shows general agreement with the predictions of the previous section. However, it should be emphasized that the theory is only qualitatively applicable since the loading in this particular case is really a
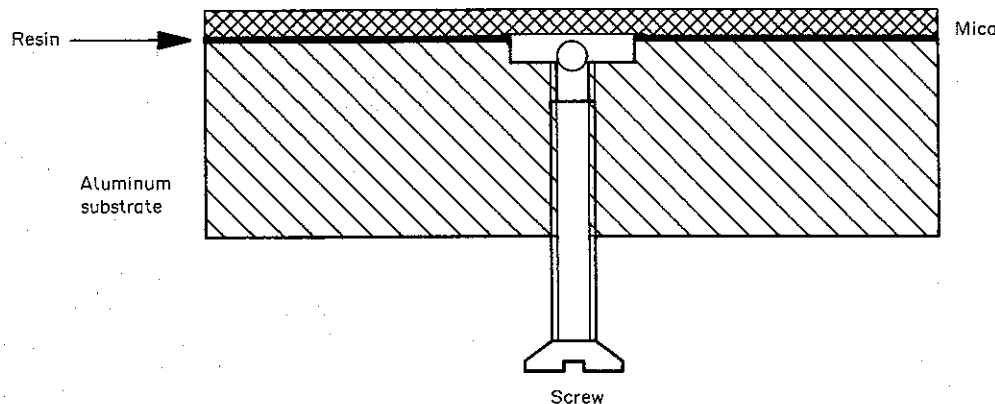

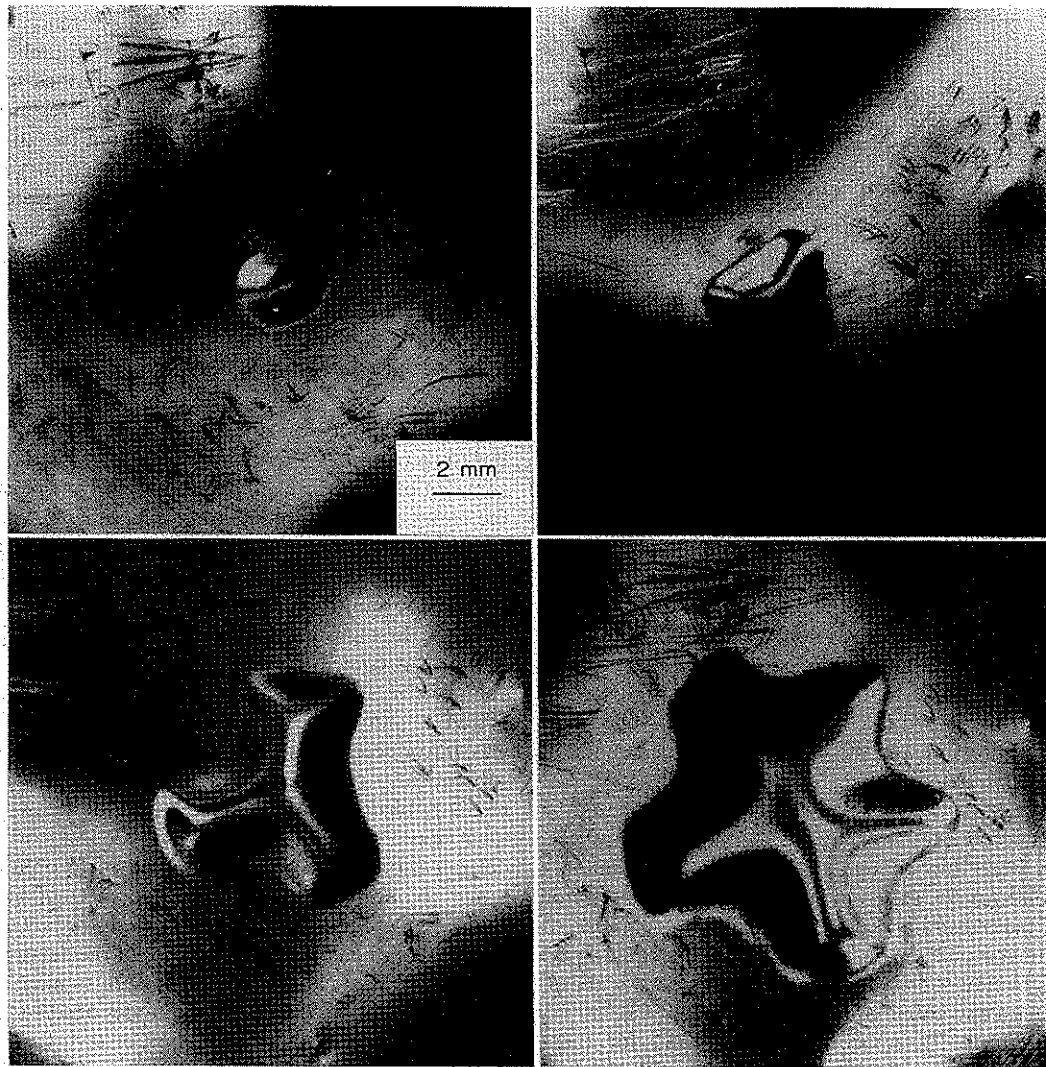Fig. 13. Geometry of the system used in the experiments.

Fig. 14. Micrographs showing the blisters resulting from the combined action of a uniform, biaxial stress
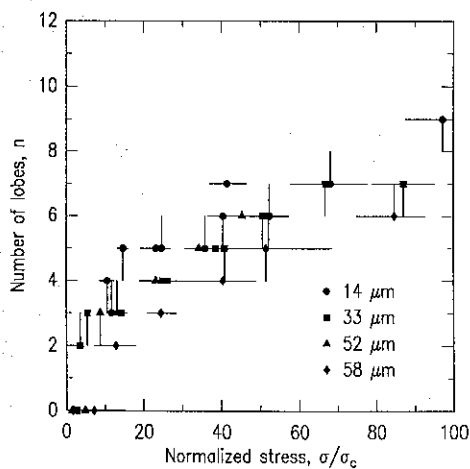and a point load.

Fig. 15. Experimental results showing the number of nodes
associated with a blister growing under a combined biaxial
stress and a point load, plotted as a function of σ/σ_c.

combination of a uniform, biaxial stress assumed in
the theory and a point load caused by the action of
the screw.

The second group of experiments was a systematic
study of the sequence of events that occur when the
stress on an initial region of delamination is in-
creased. Flaws with different initial radii were intro-
duced into the interface and, as the samples were
cooled, the events were recorded by a video camera
for further analysis. Three distinct types of behavior
were observed. First, the smallest flaws would often
cause catastrophic failure, in which the entire film
would delaminate from the substrate upon reaching
a critical temperature. A second type of behavior,
that of slightly larger flaws, is illustrated by the
sequence of photographs in Fig. 1. The blisters would
begin to extend but, as they did so, nonaxisymmetric
instabilities would develop as predicted by Section 3.
Figure 16, which shows a sequence of video images
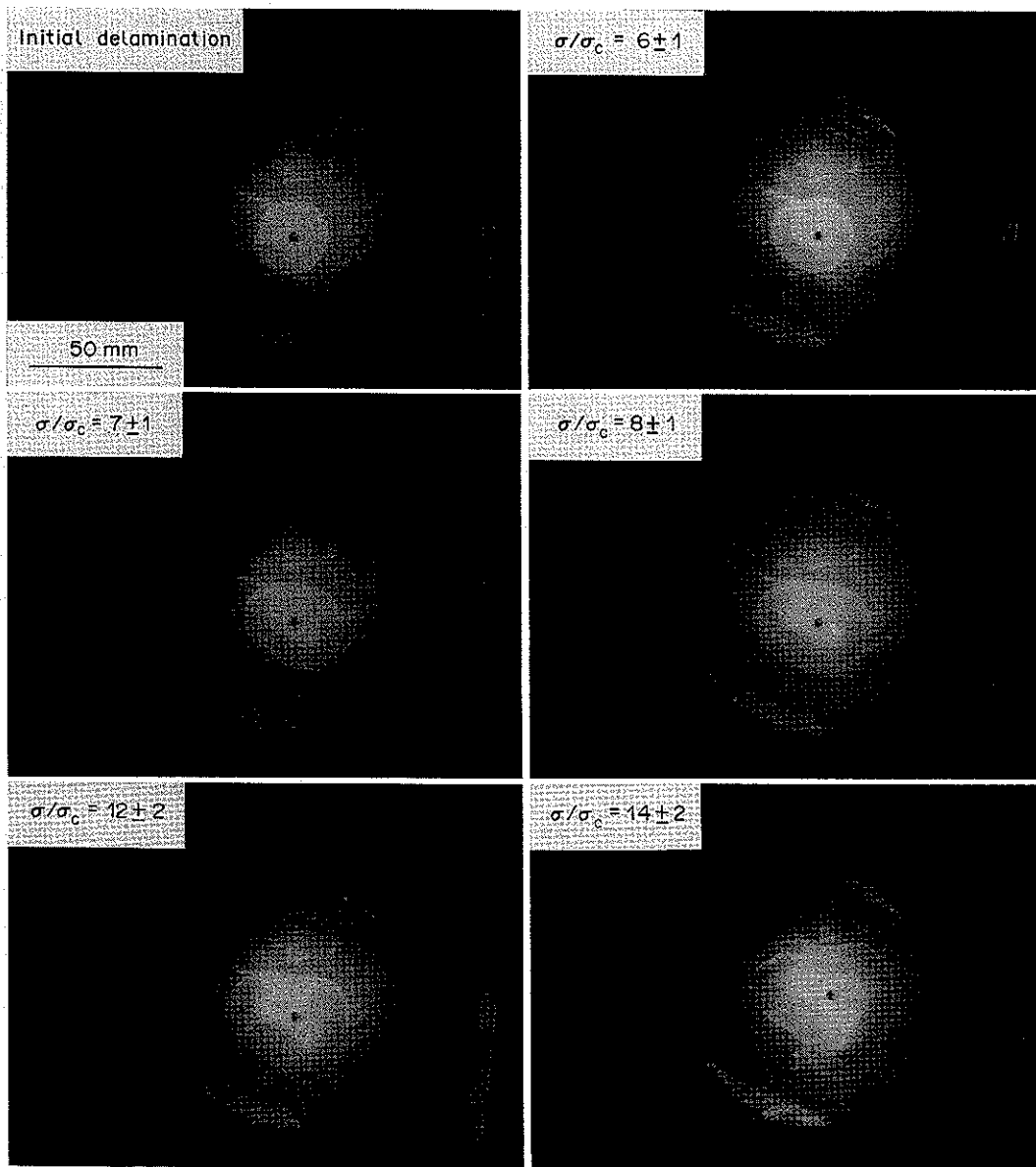for one of these samples, illustrates the development

Fig. 16. A sequence of video images showing the growth of a blister under a constant, uniform, biaxial compression. The thickness of the mica is 130 μm, and the stress in the film is about 100 MPa.

of these instabilities in more detail. However, this mechanism did not continue indefinitely; the lobes eventually developed into the "worm-like" patterns (Fig. 1) that appear to be so ubiquitous in the delamination of compressive films. Finally, a third group of relatively large blisters did not grow at all; the first indication of any activity was the extension of lobes into the "worm-like" morphologies. A summary of the conditions under which these different mechanisms were observed is given in Fig. 17.

Another goal of this work was to make some quantitative comparisons between the experiments and the theoretical discussion of the previous sections. It was emphasized in Sections 2 and 3 that the failure criterion under mixed-mode conditions has a

profound influence on the delamination behavior. Some indication of the relevant criterion is therefore required to interpret the results. Empirical fits to the interface toughness function (13) with (14) were obtained from a series of independent experiments in which mica sheets were delaminated from a similar system, but under conditions of unidirectional compression [21]. The best fit for λ was found to be about 0.3, while Γ_{1c} appeared to depend on the thickness of the mica: $\Gamma_{1c} \cong 1.7\,\text{Jm}^{-2}$ for $h \cong 130\,\mu$m, $\Gamma_{1c} \cong 0.8\,\text{Jm}^{-2}$ for $h \cong 60\,\mu$m, and $\Gamma_{1c} \cong 0.4\,\text{Jm}^{-2}$ for $h = 30\,\mu$m. Using these values as normalizing parameters, the data from Fig. 17 could then be compared to the theoretical predictions for the propagation conditions (Fig. 18). One of the more
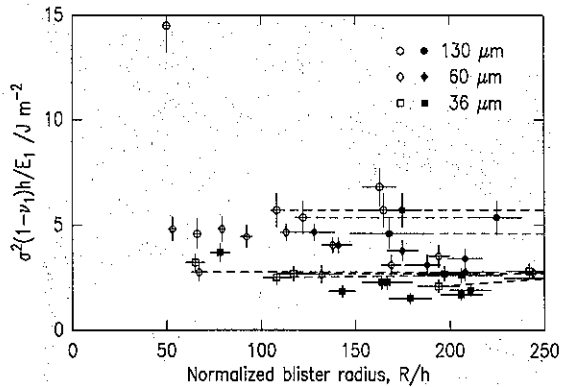
Fig. 17. Experimental results for the value of G_0 at which delamination occurred, plotted as a function of the normalized radii of the defects. The open data points correspond to the conditions at which the blisters began to expand; the solid points correspond to the conditions at which the "worm-like" morphologies developed. An isolated open point therefore corresponds to an observation of catastrophic delamination. The dashed lines connected an open point to a closed point illustrate the regions over which blisters were observed to grow.

Fig. 19. A plot of the experimental results for the number of lobes associated with a blister growing under a uniform, biaxial, compressive stress. The results compare favorably with the theoretical predictions of Section (3) appropriate for $\lambda = 0.3$.

striking features of this data is the relatively narrow range for the values of

$$\sigma\sqrt{\frac{(1-\nu_1)\bar{h}}{E_1\Gamma_{1c}}} \equiv \sqrt{\frac{G_0}{\Gamma_{1c}}}$$

required for delamination. This is in agreement with the curves of Fig. 9 in which the condition for delamination is relatively insensitive to σ/σ_c above $\sigma/\sigma_c \cong 2$.

A final comparison between the experimental observations and the theoretical predictions is shown in Fig. 19. In this figure the number of lobes in a nonaxisymmetric blister grown under the influence of a uniform, biaxial stress has been plotted as a function of the buckling parameter σ/σ_c. In contrast to the results from the blisters loaded under a combined biaxial stress and a point load, there was no obvious thickness dependence on the results. This is in agreement with the theory of Section 3; indeed, a comparison of this data with the behavior predicted for $\lambda = 0.3$ is excellent.

5. CONCLUSIONS

Two major features of buckle-driven delamination have been explored in this paper. An initial calculation developed the mechanics for the growth of an axisymmetric blister under conditions of equi-biaxial compression. A second calculation produced the important result that the crack front of such a blister can become unstable to small perturbations. Under the relevant conditions, the blister loses its axisymmetry and develops lobes around the perimeter with an order that depends on the magnitude of σ/σ_c and on the mixed mode failure criterion appropriate for the interface.

A series of model experiments were performed in conjunction with the analysis. These experiments showed excellent, quantitative agreement with the trends predicted by the theory. Furthermore, the experiments emphasized the important role that crack-front instabilities play in the development of the "worm-like" delaminations that are frequently observed in studies of thin-film delamination.
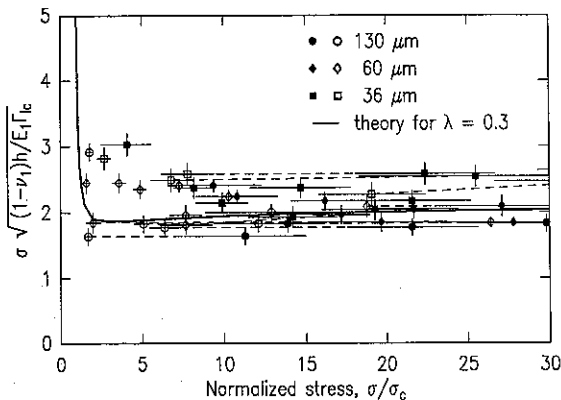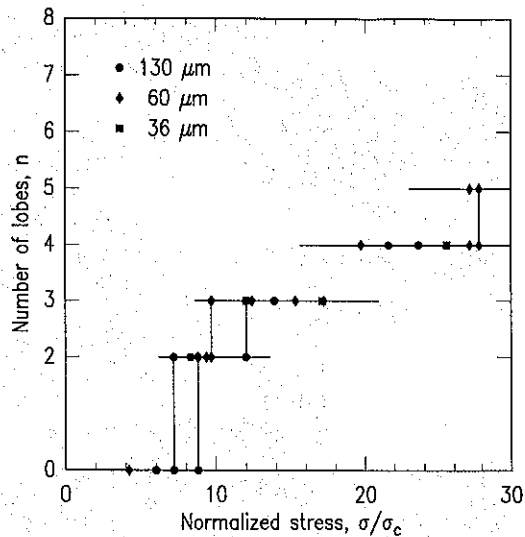
Fig. 18. A comparison of the experimental data shown in Fig. 16 with the theoretical predictions for delamination. The data has been normalized by the values of Γ_{1c} obtained from buckling experiments performed under a uniaxial compression [Ref. 21].

REFERENCES

1. G. Gille, Chap. 7, in *Current Topics in Materials Science* (edited by E. Kaldis). North Holland, Amsterdam (1985).

2. A. S. Argon, V. Gupta, H. S. Landis and J. A. Cornie, *J. Mater. Sci.* **24**, 1406 (1989).
3. D. Nir, *Thin Solid Films* **112**, 41 (1984).
4. G. A. J. Amaratunga and M. E. Welland, *J. appl. Phys.* **68**, 5140 (1990).
5. H. Chai, C. D. Babcock and W. G. Knauss, *Int. J. Solids Struct.* **17**, 1069 (1981).
6. A. G. Evans and J. W. Hutchinson, *Int. J. Solids Struct.* **20**, 455 (1984).
7. W.-L. Yin, *Int. J. Solids Struct.* **21**, 503 (1985).
8. B. Storåkers, in *Proc. 17th Int. Cong. Theor. Applied Mechanics* (edited by P. Germain, M. Piau and D. Caillerie), p. 315. Elsevier, Amsterdam (1989).
9. H. Chai, *Int. J. Fract.* **46**, 237 (1990).
10. J. D. Whitcomb, in *Composite Materials: Testing and Design* (edited by S. P. Garbo), 9th Vol., ASTM STP 1059, p. 215 (1990).
11. K. F. Nilsson and B. Storåkers, *J. appl. Mech.* To be published.
12. J. D. Whitcomb, *Comp. Sci. Technol.* **25**, 19 (1986).
13. J. W. Hutchinson and Z. Suo, in *Advances in Applied Mechanics* (edited by J. W. Hutchinson and T. Y. Wu), Vol. 29, p. 64. Academic Press, New York (1991).
14. Z. Suo and J. W. Hutchinson, *Int. J. Fract.* **43**, 1 (1990).
15. H. C. Cao and A. G. Evans, *Mech. Mater.* **7**, 295 (1989).
16. M. D. Thouless, *Acta Metall. Mater.* **38**, 1135 (1990).
17. J. S. Wang and Z. Suo, *Acta metall. mater.* **38**, 1279 (1990).
18. K. M. Liechti and Y.-S. Chai, *J. appl. Mech.* To be published.
19. J. Ahmad, *J. Engng Mater. Technol.* To be published in *J. Engng Mater. Technol.*
20. A. G. Evans and J. W. Hutchinson, *Acta metall. mater.* **37**, 909 (1989).
21. M. D. Thouless, J. W. Hutchinson and E. G. Liniger. To be published.
22. S. P. Timoshenko and J. M. Gere, *Theory of Elastic Stability*, 2nd edn. McGraw-Hill, New York (1961).
23. J. R. Fitch, *Int. J. Solids Struct.* **4**, 421 (1968).

APPENDIX

Analysis

The analysis is based on the von Karman nonlinear plate equations [22] which apply to elastic plates undergoing small strains and moderately large rotations. The analysis of the axisymmetric deformation is outlined first, followed by the nonaxisymmetric instability analysis. Standard notation for plate theory will be used.

(A1) Axisymmetric behavior

Let $D = E_1 h^3/[12(1 - v_1^2)]$ be the bending stiffness of the plate and let $x = r/R$. With $w(x)$ denoting the normal deflection and N_{rr} denoting the resultant radial in-plane stress, let

$$\phi = [6(1 - v_1^2)]^{1/2} R^{-1} w' \quad \text{and}$$

$$N = (R^2/D)[N_{rr} + \sigma h] \quad (A1)$$

where $(\ )' \equiv d(\ )/dx$. The axisymmetric buckling problem can be reduced to the following fourth order system of ordinary differential equations, written here in the standard form

$$y' = A(y)y. \quad (A2)$$

Here, $y = [\phi', \phi, N', N]$ and the *nonzero* components of the 4×4 matrix A are

$$A_{11} = -x^{-1}, \quad A_{12} = x^{-2} + (N - \sigma), \quad A_{21} = 1$$

$$A_{32} = -x^{-2}\phi, \quad A_{33} = -3x^{-1}, \quad A_{43} = 1. \quad (A3)$$

The regularity conditions at $x = 0$ are $\phi = N' = 0$ and the clamped boundary conditions at the edge of the plate are

$$\phi = 0 \quad \text{and} \quad (xN)' - v_1 N = 0 \quad \text{at} \quad x = 1. \quad (A4)$$

The nonlinear system was solved using Newton–Raphson iteration. In a given iteration the linearized system of ode's was solved by finite difference methods using a scheme very similar to that specified in some detail in [23]. For the bulk of the calculations the x-interval [0, 1] was divided into 90 integration points. Most values of quantities reported in the paper were accurate to within a small fraction of one per cent. The primary quantities of interest from the plate analysis are the moment $M = M_{rr}$ and the resultant in-plane stress change $\Delta N = N_{rr} + \sigma h$ at the edge of the plate. These quantities in (6) and (7) determine G and ψ; they are given in terms of the values of N and ϕ' at $x = 1$ by

$$\Delta N = (D/R^2)N \quad \text{and}$$

$$M = (Dh/R^2)[6(1 - v_1^2)]^{-1/2}\phi'. \quad (A5)$$

(A2) Nonaxisymmetric instability analysis

The two nonaxisymmetric analyses reported in Section 3 can be treated collectively. The problem of nonaxisymmetric buckling from the axisymmetric buckled state is an eigenvalue problem with homogeneous boundary conditions. The instability to nonaxisymmetric perturbations of the circular crack front is governed by the same differential equations, but the boundary conditions are non-homogeneous in this case. The differential equations governing nonaxisymmetric behavior are detailed first.

Let (u, v, w) denote the radial, circumferential and normal components of displacement. With ϵ as the perturbation parameter, nonaxisymmetric perturbations from the axisymmetric state $(u^{(0)}, w^{(0)})$ are sought as

$$u = u^{(0)}(r) + \epsilon u^{(1)}(r) \cos n\theta$$

$$v = \qquad + \epsilon v^{(1)}(r) \sin n\theta \quad (A6)$$

$$w = w^{(0)}(r) + \epsilon w^{(1)}(r) \cos n\theta,$$

Dimensionless displacement quantities are defined according to

$$(U, V) = (R/h^2)(u^{(1)}, v^{(1)}) \quad \text{and} \quad W = w^{(1)}/h. \quad (A7)$$

The representation (A6) is substituted into the full nonlinear von Karman plate equations and linearized with respect to ϵ. The resulting partial differential equations separate exactly in r and θ. An eighth order system of linear ordinary differential equations for U, V and W is obtained. With $Y = [W''', W'', W', W, U', U, V', V]$, that system is

$$Y' = B(y, n)Y \quad (A8)$$

where the *nonzero* components of the 8×8 matrix B are

$$B_{11} = -2x^{-1}, \quad B_{12} = (2n^2 + 1)x^{-2} + N_r^0$$

$$B_{13} = -(2n^2 + 1)x^{-3} + 12v_1\gamma^2 x^{-1} + 12\gamma\gamma'$$

$$\qquad + N_r^0 x^{-1} + N_r^{0'}$$

$$B_{14} = (4n^2 - n^4)x^{-4} - n^2 N_\theta^0 x^{-2},$$

$$B_{15} = 12v_1\gamma x^{-1} + 12\gamma'$$

$$B_{16} = 12v_1\gamma' x^{-1} + 12\gamma x^{-2},$$

$$B_{18} = 12nv_1\gamma' x^{-1} + 12n\gamma x^{-2}$$

$$B_{21} = 1, \quad B_{32} = 1, \quad B_{43} = 1, \quad B_{52} = -\gamma$$

$$B_{53} = -\gamma' - (1 - v_1)\gamma x^{-1},$$

$$B_{54} = (1 - v_1)n^2\gamma x^{-2}/2, \quad B_{55} = -x^{-1}$$

$$B_{56} = [1 + (1 - v_1)n^2/2]x^{-2},$$

$$B_{57} = -(1 + v_1)nx^{-1}/2$$

$$B_{58} = (3 - v_1)nx^{-2}/2, \quad B_{65} = 1,$$

$$B_{73} = [(1 + v_1)/(1 - v_1)]n\gamma x^{-1}$$

$$B_{74} = n\gamma x^{-2} + n\gamma' x^{-1},$$

$$B_{75} = [(1 + v_1)/(1 - v_1)]nx^{-1}$$

$$B_{76} = [(3 - v_1)/(1 - v_1)]nx^{-2}, \quad B_{77} = -x^{-1}$$

$$B_{78} = [2/(1 - v_1)]n^2 x^{-2} + x^{-2}, \quad B_{87} = 1. \quad (A9)$$

Here, γ, N_r^0 and N_θ^0 are quantities from the nonlinear axisymmetric solution defined by

$$\gamma = [6(1 - v_1^2)]^{-1/2} \phi$$

$$N_r^0 \equiv (R^2/D)N_{rr} = N - \sigma R^2 h/D$$

$$N_\theta^0 \equiv (R^2/D)N_{\theta\theta} = N_r^0 + xN_r^{0'}. \qquad (A10)$$

The conditions which must be imposed at $x = 0$ are $U = V = W = W' = 0$ for all $n \geqslant 2$. For $n = 1$, the pole conditions are $U + V = 0$, $U' + V' = 0$, and $W = W'' = 0$.

The boundary conditions at the edge of the plate ($x = 1$) for the *nonaxisymmetric buckling problem* are $U = V = W = W' = 0$. These homogeneous conditions, together with the homogeneous conditions at $x = 0$, give rise to an eigenvalue problem for the lowest stress σ at which non-axisymmetric buckling from the nonlinear axisymmetric state first occurs. The eigenvalue search was conducted numerically using standard methods coupled with a finite difference solution procedure for the system (A8). As reported in Section 3, for $v_1 = 1/3$ the lowest eigenvalue found was $\sigma/\sigma_c = 55.6$ associated with $n = 8$.

For the analysis of *instability to nonaxisymmetric pertuba-tions of the circular crack front*, clamped boundary conditions are imposed on the plate on its perturbed edge (21)—see also Fig. 2(b). When these conditions are expanded in ϵ, the boundary conditions at the edge of the plate governing the lowest order perturbation solution become (at $x = 1$)

$$u^{(1)} = -u^{0'}, \quad v^{(1)} = w^{(1)} = 0 \quad \text{and} \quad w^{(1)'} = -w^{0''}. \quad (A11)$$

These can be re-expressed as

$$U = -N/12, \quad V = W = 0 \quad \text{and}$$

$$W' = -\gamma' \quad \text{at} \quad x = 1. \quad (A12)$$

Equation (A8) together with the boundary conditions at $x = 0$ and those above at $x = 1$ specify the lowest order nonaxisymmetric perturbation. The system equations were solved using the same scheme which was employed in the numerical analysis of the linear ode's in the axisymmetric problem.

Stability of the circular crack front to nonaxisymmetric perturbations depends on the sign of F_1 as discussed in Section 3. The derivation of F_1 in terms of the perturbation solution is now given. By (15)

$$dF = f^{-1} dG - f^{-2}G(df/d\psi) d\psi \qquad (A13)$$

where by (6) and (7)

$$dG = D^{-1}[M dM + (h^2/12)\Delta N d\Delta N]$$

$$d\psi = -d[h\Delta N/(\sqrt{12}M)] \cdot [-\sin \omega$$
$$+ (h\Delta N/(\sqrt{12}M))\cos \omega]^{-2}.$$

As footnoted earlier, the mode 3 contribution to dG can be shown to vanish, to lowest order in ϵ. The terms $\epsilon F_1 \cos n\theta$ in (22) can be identified with dF in (A13) when F is perturbed using the expansion (A6). The final expression for F_1 is obtained as

$$F_1 = f^{-1}G_1 - f^{-2}G(df/d\psi)\psi_1 \qquad (A14)$$

where

$$G_1 = D^{-1}[MM_1 + (h^2/12)\Delta N\Delta N_1]$$

$$\psi_1 = -(h/\sqrt{12})\{1 + [h\Delta N/(\sqrt{12}\,M)]^2\}^{-1}$$
$$[M\Delta N_1 - \Delta NM_1]M^{-2}$$

$$M_1 = (Dh/R^2)[W'(1) + W''(1)]$$

$$\Delta N_1 = 12(D/R^2)[U(1) + U'(1)].$$

The quantities other than M_1 and ΔN_1 in the expressions for F_1, G_1 and ψ_1 are all evaluated in the axisymmetric state.